Frequency-Domain Differential Phase Shift Keying in Femtosecond Spread-Time WDM/TDM Systems

J.-K. Rhee†, M. Dugan†, J. X. Tull†, H. Kobayashi,* and W. S. Warren†
Center for Photonics and Opto-Electronic Materials, Princeton University, Princeton, New Jersey 08544
† *Department of Chemistry, Princeton University, Princeton, New Jersey 08544*
* *Department of Electrical Engineering, Princeton University, Princeton, New Jersey 08544*

Abstract

We propose a fiber optic WDM/TDM communication network architecture employing an acoustooptic modulator in a femtosecond pulse shaper. Using the pulse shaper and <100-fs optical pulses, we can multiplex 1000 WDM channels in a 200-ps time window, corresponding to a 5-Tbps aggregate transmission throughput. Taking advantage of coherence between different WDM channels, we can implement frequency-domain differential phase shift keying (FD DPSK). We also propose appropriate designs of receivers capable of simultaneous TDM channel drop and FD DPSK detection.

I. Introduction

The typical bandwidths (~10 THz) of commercially available single mode fibers, fiber amplifiers, and femtosecond lasers make it possible in principle to achieve terabits-per-second (Tbps) optical fiber communications. By definition, encoding information on an optical carrier requires pulse shaping; an unshaped optical wave (no amplitude, frequency, or phase modulation) or a simple modelocked pulse train carries no information. Rapid information transmission (risetime Δt) implies large frequency bandwidths (Δf), in accord with the classical time-bandwidth uncertainty relation $\Delta f \Delta t \approx 1$. New developments in rapid optical modulation capabilities give the potential for an order of magnitude improvement in communications bandwidths over existing systems. In this paper, we discuss a new pulse shaping method (using an acousto-optic modulator (AOM) to implement dense amplitude and phase coding in the spatio-spectrum domain) which can modulate a 100-fs pulse with >1000-pixel spectral resolution, and can be updated rapidly. We discuss possible architecture for Tbps WDM/TDM for short-haul fiber communication systems based on this method. This application of femtosecond pulse shaping allows coherent optical communication, since all wavelength components are phase locked to one another. We also introduce an optical frequency-domain differential phase shift keying scheme (FD DPSK) and relevant receiver designs for applications in the femtosecond-pulse WDM/TDM optical communication network, which show better noise-filtering properties.

II. Terabits-per-second WDM/TDM System

At first glance, subpicosecond resolution laser pulse shaping sounds both impossible (no existing optical modulators have such a rapid risetime) and impractical (even if you had a sub-picosecond modulator, where would you get shaped voltage pulses to drive it?). The first laser multiple pulse sequence with non-overlapping pulses and a completely controlled phase shift between pulses was demonstrated in 1981 [1], and then only with nanosecond resolution and low powers. However, phase shifting technology rapidly evolved in the 1980s into the femtosecond time domain [2-4]. In addition, programmable pulse shaping capabilities evolved from ≈4 ns resolution with pieces chopped out of a continuous laser [5] to <100 fs time resolution with amplified pulses [6-8].

Reference [9] reported the development of a method for modulating femtosecond laser pulses using *microsecond* rf pulses in an acousto-optic modulator (AOM) in the pulse shaping apparatus illustrated in Fig. 1. An ultrafast laser pulse is dispersed by a diffraction grating, then collected with a focusing lens. Then a spatially dispersed spectrum of the laser pulse is imaged as a line in the focal plane. The pulse then passes through an acousto-optic modulator (AOM). A shaped radiofrequency (rf) pulse then drives the AOM's transducer, creating a shaped acoustic waveform traveling through the crystal. The beam deflection by the modulator is ≈20 mrad. It then passes through a second lens, and a second grating recombines the different colors. The maximal number of acoustic waveform features is the time aperture product, obtained by multiplying the acoustic wave transit time by the inverse of the risetime. Experiments with near-IR (800 nm) 100-fs pulses from a modelocked Ti:sapphire oscillator

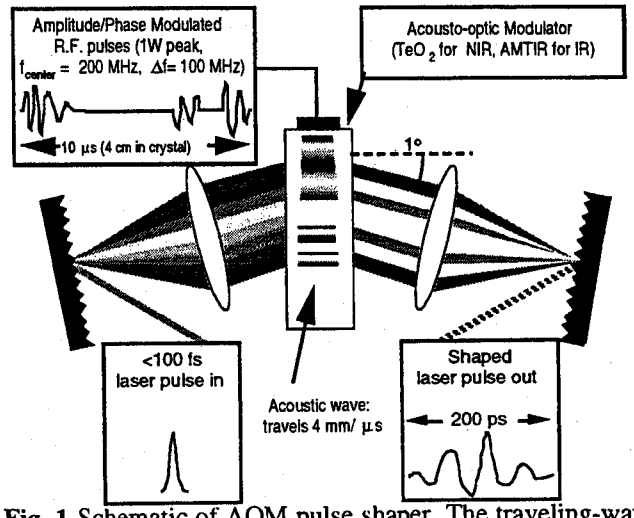

Fig. 1 Schematic of AOM pulse shaper. The traveling-wave AOM is placed at the focal line of a zero-dispersion line consisting of a pair of gratings and lenses.

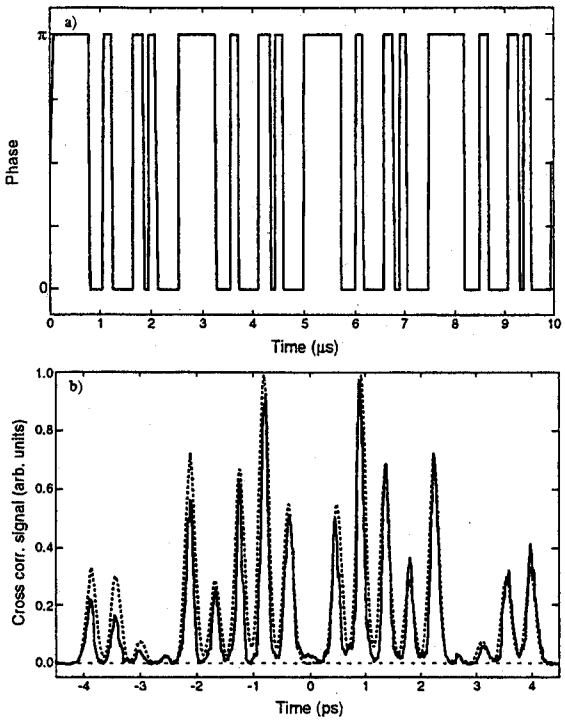

Fig. 2 An experimental example of binary phase modulation with the AOM pulse shaper; the applied rf waveform, (a), and the corresponding temporal profile of the shaped femtosecond pulse.

achieved a maximum resolution equivalent to >1000 effective pixels, employing a 4-cm tellurium-dioxide (TeO_2) AOM which has a 10-μs aperture time and 100-MHz modulation bandwidth. Fig. 2 shows a specific example, in this case employing pure phase modulation.

In general, an optical shaped pulse with N bits of spectral encoding will be approximately N times longer than a transform-limited pulse, thus spread in time. For example, modulation of a 200-fs optical pulse with 1000-bit resolution will produce the transmission signal spread in 200-ps time interval. This spread-time (ST) WDM signal is then allocated to a TDM slot. In contrast, in traditional WDM/TDM, each wavelength component starts from a relatively long pulse width (e.g.. 200 ps) and has no phase correlation with any other.

The STWDM permits data transmission with very high data rates. For example, suppose we had an AO modulator with 1-GHz bandwidth, which would permit about 1000 bits of binary (amplitude- or phase-modulated) data in 1 μs. Then an STWDM signal would be generated from a 200-fs input laser pulse, occupying in the time for 200 ps. Another laser pulse arriving 1 μs later could see a completely different data stream in the AOM; thus one laser pulse per μs would give a data rate of 1 Gbps, yet the communication channel would be dark for all but 200 ps each 1μs (0.2% duty cycle). Therefore, TDM could produce an effective throughput of ≈5 Tbps, ignoring practical issues such as gaps between channels, cross-talking between different wavelength components, bit error rates; Even inclusion of such considerations would still permit design of robust architecture with data rates far in excess of modern commercial systems.

III. Frequency-Domain DPSK

Using the AOM to produce spectral phase modulation (as in Fig. 2) could provide a significant advantage over amplitude modulation, since an amplitude modulated binary data stream will discard, on the average, 50% of the initial system energy. In addition, stronger rf. pulses (which produce some deviations from linear response in the diffraction efficiency per watt) can then be used for a higher modulation efficiency. However, the common detection devices in optics (photodiodes and photo-multiplier tubes) measure only the intensity, discarding phase information.

In the STWDM case, the signal has well defined phase relations between the different wavelength components. Here we develop a novel frequency-domain differential-phase-shift-keying (FD DPSK) scheme, which utilizes such phase coherence. This scheme eliminates the requirement of phase reference or local oscillator of traditional coherent optical communication systems.

Consider an n-channel network system whose key sequence is given by $\{a_1,..,a_n\}$, $a_i \in \{0,..,m-1\}$, where m is a positive integer; in what follows we explicitly consider the binary case ($m=2$). The corresponding DPSK sequence $\{\phi_0,..,\phi_n\}$ is defined by the following relation:

$$\phi_i = \begin{cases} 0, & \text{for } i=0, \quad (1a) \\ \psi(a_i)+\phi_{i-1}, & \text{for } i=1,..,n, \quad (1b) \end{cases}$$

where

$$\psi(a_i) = \arccos(1-2a_i). \quad (2)$$

Ordinarily DPSK is implemented in TDM channels in radio-frequency (rf) communication systems. However, in our frequency-domain DPSK, the differential phase is encoded in each wavelength channel of the STWDM system. The differential phase is later retrieved by interfering adjacent STWDM chips by means of a frequency shift.

For such a frequency-domain DPSK system, we use fs lasers to generate the coherent STWDM signal. First consider the spectrum of a transform-limited ultrashort optical pulse. For simplicity we assume a rectangular spectrum with spectral bandwidth $\Delta\omega$ and amplitude 1, but the idea is more general. The spectrum is then divided into $(n+1)$ chips for STWDM:

$$\tilde{E}_m(\omega) = \sum_{i=0}^{n} \mathrm{rect}(\omega-\omega_i, \delta\omega)\exp(j\phi_i), \quad (3)$$

$$\mathrm{rect}(x,a) = \begin{cases} 1, & \text{for } -|a|/2 \le x \le |a|/2 \\ 0, & \text{otherwise,} \end{cases} \quad (4)$$

where $\tilde{E}_m(\omega)$ is the (complex) amplitude of the optical pulse as a function of frequency ω. The central frequency and the bandwidth of the i-th chip are given by $\omega_i =$

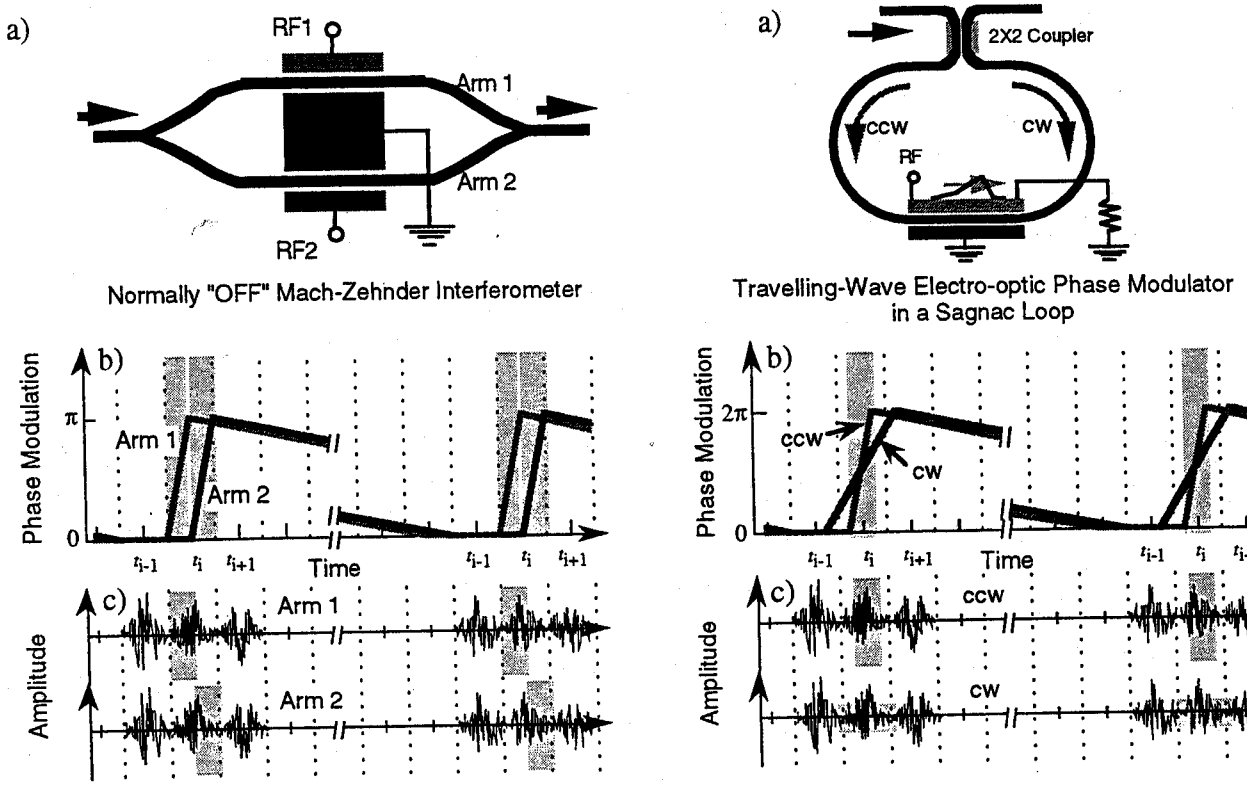

Fig. 3 Schematic of Mach-Zehnder receiver, (a), and the operation principle, (b) and (c). The receiver consists of a pair of fast electro-optic modulators. Radio-frequency voltages (RF1 and RF2) are applied to produce phase modulation on each arm as shown in figure (b). Shaded regions of figure (c) indicate the corresponding frequency-shift windows for the light traveling in Arm1 and Arm2.

Fig. 4. Schematic of a Sagnac receiver, (a), and the operation principle, (b) and (c). The receiver consists of a fast traveling-wave electro-optic modulators. Radio-frequency voltage (RF) is applied to produce phase modulation on each traveling direction as shown in figure (b). Shaded regions of figure (c) indicate the corresponding frequency-shift windows for each traveling direction.

$\omega_0 + \delta\omega\, i$ and $\delta\omega = \Delta\omega/(n+1)$, respectively, where ω_0 is the central frequency of the longest wavelength chip. The receiver may consist of either a Mach-Zehnder or a Sagnac interferometer with a relevant device for shifting the optical frequency by $+\delta\omega$ on one arm, and an n-channel spectrum analyzer with $\delta\omega$ resolution at the detector. After the frequency shift, the $(i-1)$-th component will have the same central frequency as that of i-th component:

$$\tilde{E}_{i-1}^{+\delta\omega}(\omega) = \mathrm{rect}(\omega - \omega_i, \delta\omega)\exp(j\phi_{i-1} + j\Delta) \qquad (5)$$

Here Δ is the phase difference in the transmission direction between the two arms of the interferometer; for a normally-off receiver, we take $\Delta = \pi$. Then, the i-th STWDM chip on the detector can be obtained using $\psi(a_i) = \phi_i - \phi_{i-1}$:

$$I_i^{\mathrm{det}}(\omega) = \frac{1}{2}\mathrm{rect}(\omega - \omega_i, \delta\omega)\left[1 - \cos(\psi(a_i))\right], \qquad (6)$$

for $1 \le i \le n$.

Thus the phase information is converted to intensity modulation, and the original sequence is directly retrieved from the DPSK sequence.

IV. FD DPSK Receivers

Optical frequencies can be shifted by electro-optic (EO) modulators, four-wave mixing (FWM), wavelength conversion in semiconductor optical amplifiers (SOA), and AOMs. The frequency shift must preserve phase information and be large enough to be resolved by optical spectrometer for a practical system. However, FWM reverses the frequency order of WDM channels, wavelength conversion in an SOA is noncoherenct process, and existing AOMs are not capable of such frequency shift. Thus, a synchronized EO modulator is a good choice. We incorporate TDM channel drop in the FD DPSK receivers by gating the frequency shift in the time domain. One can easily implement such receivers with Mach-Zehnder and Sagnac interferometers.

In Fig. 3(a), the input FD DPSK light signal is split into Arm 1 and Arm 2 of a normally-off waveguide Mach-Zehnder interferometer. We apply ramp radio-frequency biases to the modulators, sweeping from 0 to π phase shift during a $\pi/\delta\omega$ period. Thus we introduce a $\delta\omega$ frequency shift. As shown in Fig. 3(b), the phase modulation of Arm 1 leads that of Arm 2 by $\pi/\delta\omega$, in order to produce interference between the frequency-shifted and unshifted light signals. The first half of the light signal traveling in Arm 1 is frequency shifted and the corresponding part of Arm 2 is not; in the second half, Arm 2 is frequency shifted and the corresponding part of Arm 1 is not. As a result, we produce the desired interference of the two light signals at the output side of the Mach-Zehnder interferometer. Analyzing the spectrum of the output

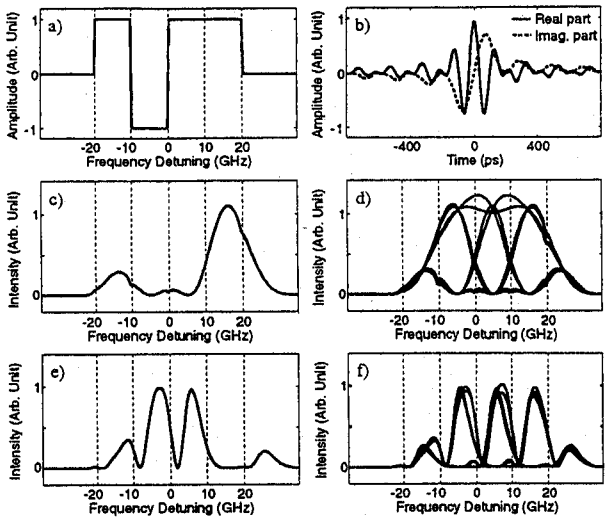

Fig. 5 Simulation data for a typical FDDPSK signal, (a) and (b), and output specrta of a Mach-Zehnder receiver, (c) and (d), and a Sagnac receiver, (e) and (f).

gives a spectral intensity modulation given by Eq. (6). Subsequently, the modulator bias voltage relaxes with a sufficiently slow time constant to keep the relative phase of the two arms nearly the same. Thus, there is no output light during the relaxation period in the normally-off Mach-Zehnder; the frequency-shift and interference take place only during a given TDM time slot.

In a similar way, one can implement a Sagnac receiver by taking advantage of a traveling-wave waveguide EO phase modulator. The schematic of the Sagnac receiver is shown in Fig. 4(a). The Sagnac fiber loop acts as a mirror due to destructive interference, in transmission, between clockwise (cw) and counter-clockwise (ccw) traveling light, when lights traveling in both directions experience exactly the same phase variation. However, a fast rf bias voltage to the traveling-wave EO phase modulator introduces different phase modulations in each direction, as shown in Fig. 4(b)–the co-propagating (ccw) light experiences fast modulation, and counter-propagating (cw) light experiences slow one. The light signals in both directions are frequency shifted, but by different degrees. (The heights of the shaded regions in Fig. 4(c) indicate degrees of the frequency shift.) When the difference of the frequency shift between the two directions is $\delta\omega$, the FD DPSK is converted to an amplitude modulation in the transmission direction of the Sagnac loop. Of course, this receiver is also capable of TDM channel drop because ccw and cw light signals experience almost the same phase shift outside the TDM chip of interest.

V. Modeling and Computer Analysis

Performance of FD DPSK receivers is, of course, dependent on selection of operational parameters such as the slope and the maximum voltage of the rf ramp bias. The optimal parameters can be obtained by computer simulations. In addition, it is interesting to examine how robust the FD DPSK is to noise, compared with amplitude shift keying. In this section, we model the Mach-Zehnder and Sagnac receivers and show the functionality of the receivers. Then we analyze the noise characteristics of our FD DPSK STWDM/TDM system.

V.1 Mach-Zehnder FD DPSK receiver

Because we apply time-varying rf biases to the electro-optic modulators (Fig. 3), we consider time-domain input light signal modulated with FD DPSK. The time-domain signal $E_m(t)$ is obtained by a Fourier transform of $\tilde{E}_m(\omega)$. In the Mach-Zehnder interferometer, the signal is split into the two arms and combined to produce interference. In the normally off state, the signals traveling in Arm1 and Arm2 are represented as $+\frac{1}{2}E_m(t)$ and $-\frac{1}{2}E_m(t)$, respectively. As applying rf biases to the electro-optic modulators as depicted in Fig. 3(b), we obtain the output signal of the Mach-Zehnder interferometer as follows:

$$E_{\mathrm{dem}}(t)=\frac{1}{2}E_{\mathrm{m}}(t)\exp\left(j\delta\omega T_{\mathrm{r}}\mu(t+T_{\mathrm{r}}/2)\right) - \frac{1}{2}E_{\mathrm{m}}(t)\exp\left(j\delta\omega T_{\mathrm{r}}\mu(t-T_{\mathrm{r}}/2)\right), \qquad (7)$$

where the phase modulation function is given by

$$\mu(t)=\left(\frac{1}{2}+\frac{t}{T_{\mathrm{r}}}\right)\mathrm{rect}(t,T_{\mathrm{r}}) + \left(\frac{1}{2}-\frac{t-t_{\mathrm{f}}}{T_{\mathrm{f}}}\right)\mathrm{rect}(t-t_{\mathrm{f}},T_{\mathrm{f}}). \qquad (8)$$

Here T_{r} and T_{f} are the rise and fall times of a triangle-shaped function with a sharp rise edge and a slow fall tail $(T_{\mathrm{r}}<<T_{\mathrm{f}})$, and $t_{\mathrm{f}}=(T_{\mathrm{r}}+T_{\mathrm{f}})/2$. In the rise edge, the frequency shift due to phase sweep is $\delta\omega$, which is a parameter designated in the network design. Thus we have degree of freedom in choosing T_{r}; the choice of different T_{f} values has little effect on the receiver operation. Fourier transforming the demodulated time-domain signal $E_{\mathrm{dem}}(t)$, we finally obtain the power spectrum for the original data sequence $\{a_i\}$.

We have computer simulated our model for a three-channel case ($n=3$) to find an optimal choice of T_{r} and to study noise characteristics of the FD DPSK system. We assume $\delta\omega/2\pi$=10 GHz, which corresponds to a 0.08-nm spectral resolution at 1.55 μm. Fig. 5 shows a typical example ($\{a_i\}=\{1,1,0\}$) of FD DPSK spectral amplitude signal, (a), the corresponding spread-time amplitude signal, (b), and the power spectrum demodulated by the receiver, (c). Here we find T_{r}=55 ps for the maximal discrimination between '0' and '1.' Interestingly, the Mach-Zehnder receiver produces the *inverted image* of the data sequence in the case of normally-off operation. In figure (d), we simulated an "eye diagram" for the noise-free case to show how the receiver works. The eye diagram is generated plotting the power spectra of the receiver outputs for all possible eight cases of $\{a_i\}$ sequence.

V.2 Sagnac FD DPSK receiver

Employing a traveling-wave electro-optic modulator in a Sagnac fiber loop allows for interference between adjacent frequency components, thus FD DPSK demodulation. In modeling such a Sagnac receiver, we first consider the phase modulation of co- and counter- propagating lights in a traveling-wave electro-optic modulator. Consider the instantaneous refractive index modulation which is proportional to the traveling rf electric field in the wave-guide electrode in Fig. 4. The phase modulation can be represented as

$$\Delta\phi = k_0 \int_0^L \Delta n_{\max} \mu(t' - x/c)dx, \qquad (9)$$

where L is the length of the waveguide electro-optic modulator, $n_{\max}$ is the index modulation depth, $\mu(t)$ is defined in Eq. (8), k_0 is the magnitude of the wave vector in the free space, and c is the speed of the traveling rf field which is matched to the speed of light in the wave guide. We assume here that the rf modulation electric field is launched at $x = 0$, and travels to the other end of the wave guide modulator at $x = L$. Light field launched at time t and traveling in the same direction interacts with the portion of the modulation field at $t' = t + x/c$. Thus Eq. (9) becomes

$$\Delta\phi_{co}(t) = k_0 L \Delta n_{\max} \mu(t), \qquad (10)$$

for co-propagating light field. Here we define $\delta\omega_{Sag}$ as in $\delta\omega_{Sag} T_R = k_0 L \Delta n_{\max}$, i.e. the slope of phase variation in the rise edge. For light field launched at $x = L$ and traveling in the opposite direction, $t' = t + (L - x)/c$. Eq. (9) is then evaluated as

$$\Delta\phi_{counter}(t) = k_0 \int_0^L \Delta n_{\max} \mu(t + (L - 2x)/c)dx \qquad (11)$$

$$= k_0 \Delta n_{\max} \int_{-\infty}^{+\infty} \mathrm{rect}(x, L)\mu(t - 2x/c)dx, \qquad (12)$$

for counter-propagating light field. As we can see, the modulation speed of counter-propagating light field decreases with L when $T_R < L/c$. The rise time of $\phi_{counter}(t)$ is $\sim L/c$, i.e. the transit time of the traveling wave modulator. Thus the frequency shift near $t = 0$ is $ck_0\Delta n_{\max}$, or $\delta\omega_{Sag} T_R c/L$. In order to achieve interference between each pair of adjacent STWDM chips, (i-1)-th chip in the co-propagation direction ought to have the same central frequency as that of i-th chip in the counter-propagation direction. Therefore, we should select $\delta\omega_{Sag} = (1 - T_R c/L)^{-1}\delta\omega$. Note that the center of the modulator wave guide should coincide with the center of the Sagnac loop in order to have the same modulation timing for light signals in both co- and counter-propagation directions.

Since a Sagnac loop is normally-off in the transmission port, the signals traveling in the ccw and cw directions are also regarded as $+\frac{1}{2}E_m(t)$ and $-\frac{1}{2}E_m(t)$, respectively. Finally, we find the demultiplexed and demodulated signal:

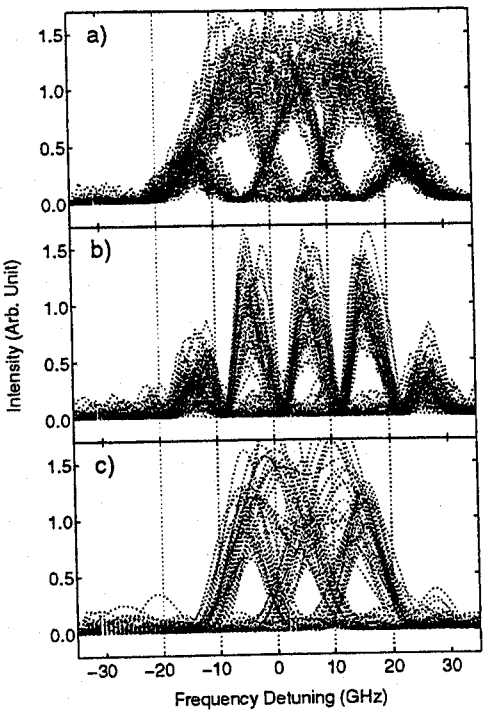

Fig. 6 Eye diagrams for a signal-to-noise ratio of 1; (a) for Mach-Zehnder receiver, (b) for Sagnac receiver, and (c) for conventional amplitude modulation case.

$$E_{dem}(t) = \frac{1}{2}E_m(t)\exp\left(j\phi_{co}(t)\right) - \frac{1}{2}E_m(t)\exp\left(j\phi_{counter}(t)\right). \qquad (15)$$

Similarly to the analysis of Mach-Zehnder case, we obtain the power spectrum for the original data sequence $\{a_i\}$ by Fourier transforming the demodulated time-domain signal $E_{dem}(t)$.

Fig. 5 also shows computer simulation data for the Sagnac loop design. Figures (e) and (f) show the demodulated receiver output power spectrum corresponding to the same data sequence $\{a_i\} = \{1,1,0\}$ and the eye diagram for noise-free signals, respectively. In contrast to Mach-Zehnder case, the demodulated signal is not inverted. We used T_r=100 ps and $\delta\omega_{Sag}/2\pi$=12 GHz, for the maximal discrimination between '0' and '1.' The data clearly shows the capability of conversion from FD DPSK to an amplitude-modulated power spectrum.

V.3 Noise characteristics of FD DPSK receivers

Phase shift keying is generally less sensitive to noise than is amplitude shift keying, which permits higher fidelity of the network. In FD DPSK receivers, the frequency shift acts as an additional noise filter discriminating against random phase and amplitude fluctuations. As a result, the FD DPSK scheme demonstrates extremely high noise fidelity. In this section, we simulate and compare the noise characteristics of cases for FD DPSK and ASK.

In Fig. 6, we present simulated eye diagrams of the receiver power spectrum output for (a) FDDPSK with a Mach-

Zehnder receiver, (b) FDDPSK with a Sagnac receiver, and (c) ASK. The input data sequences are generated randomly, and random noise is added to the signals in the time domain with signal to noise ratios of 1. We use the same system parameters as in the previous sections for FD DPSK receivers. For a fair comparison, the ASK receiver output signal is obtained after the TDM channel drop (we time gate the noisy ASK signals with the same temporal 100 ps window size as for FD DPSK). The eye diagrams show clear enhancement of the noise characteristics in the FDDPSK Mach-Zehnder receiver.

VI. Conclusion

We introduce a novel *frequency-domain differential phase shift keying* for use in femtosecond spread-time WDM systems. In contrast to a traditional coherent optical communication systems, the FD DPSK requires neither reference phase nor local oscillators. Therefore, FD DPSK allows for a simple noise-robust system for coherent optical communications, because the capability of phase shift keying combined with amplitude shift keying increases the network throughput by a multiple fold.

We also propose *FD DPSK receiver designs* capable of TDM channel drop and FD DPSK demodulation simultaneously. These receivers consist of electrooptic phase modulators and either a Mach-Zehnder interferometer or a Sagnac interferometer. The operation schemes of these receivers employ novel ideas for simultaneous frequency shift and time gating.

We demonstrated the operation principles of both Mach-Zehnder and Sagnac receivers with quantitative computer simulations. The results show outstanding capability of TDM channel drop and demultiplexing of a FDDPSK signal. In particular, a Mach-Zehnder receiver demonstrates outstanding noise elimination, which would make in an excellent candidate for future use in optical coherent communication systems.

References

[1] W. S. Warren and A. H. Zewail, J. Chem. Phys., vol. 75, p. 5856, 1981.

[2] A. Mukherjee, N. Mukherjee, J.-C. Diels, and G. Arzumanyan, in *Ultrafast Phenomena V* (Springer-Verlag, Berlin), p.266, 1986.

[3] N. F. Scherer, A. J. Ruggiero, M. Du, and G. R. Fleming, J. Chem. Phys., vol. 93, p. 856, 1990.

[4] F. Spano, M. Haner, and W. S. Warren, Chem. Phys. Lett., vol. 135, p. 97, 1987; W. S. Warren and M. Haner, in *Atomic and Molecular Processes with Short Intense Laser Pulses* (Plenum, New York), vol. p.1, 1988.

[5] C. P. Lin, J. Bates, J. Mayer, and W. S. Warren, Chem. Phys., vol. 86, p. 3750, 1987.

[6] M. Haner, and W. S. Warren, in*Ultrafast Phenomena VI* (Springer, Berlin), p.139, 1988.

[7] A. M. Weiner, R. N. Thurston, W. J. Tomlinson, J. P. Heritage, D. E. Leaird, and E. M. Kirschener, Opt. Lett., vol. 14, p. 326, 1989.

[8] A. M. Weiner, D. E. Leaird, J. S. Patel, and J. R. Wullert, Opt. Lett., vol. 15, p. 326, 1990.

[9] C. W. Hillegas, J.X. Tull, D. Goswami, D. Strickland, and W.S. Warren, Opt. Lett., vol. 19, p. 737, 1994; J. X. Tull, M. A. Dugan, and W. S. Warren, to be printed in Advances in Magnetic and Optical Resonance, vol. 20, 1996.